Transient response of fluid pressure in a poroelastic material under uniaxial cyclic loading

AUTHOR(S):

Kameo, Yoshitaka; Adachi, Taiji; Hojo, Masaki

CITATION:

Kameo, Yoshitaka ...[et al]. Transient response of fluid pressure in a poroelastic material under uniaxial cyclic loading. Journal of the Mechanics and Physics of Solids 2008, 56(5): 1794-1805

ISSUE DATE:

2008-05

URL:

http://hdl.handle.net/2433/88946

Transient response of fluid pressure in a poroelastic material under uniaxial cyclic loading

Yoshitaka Kameo[a], Taiji Adachi[a, b], and Masaki Hojo[a]

a: Department of Mechanical Engineering and Science, Kyoto University
b: Computational Cell Biomechanics Team, VCAD System Research Program, RIKEN

Corresponding author:	Taiji Adachi, ph.D.
Mailing Address:	Department of Mechanical Engineering and Science
	Kyoto University
	Yoshida-honmachi, Sakyo, Kyoto 606-8501, Japan
Telephone & Fax:	+81 (75) 753-5216
E-mail:	adachi@me.kyoto-u.ac.jp

Submitted to “Journal of the Mechanics and Physics of Solids” on August 20th, 2007

Abstract

Poroelasticity is a theory that quantifies the time-dependent mechanical behavior of a fluid-saturated porous medium induced by the interaction between matrix deformation and interstitial fluid flow. Based on this theory, we present an analytical solution of interstitial fluid pressure in poroelastic materials under cyclic uniaxial loading. The solution contains transient and steady-state responses. Both responses depend on two dimensionless parameters: the dimensionless frequency Ω that stands for the ratio of the characteristic time of the fluid pressure relaxation to that of applied forces, and the dimensionless stress coefficient H governing the solid-fluid coupling behavior in poroelastic materials. When the phase shift between the applied cyclic loading and the corresponding fluid pressure evolution in steady state is pronounced, the transient response is comparable in magnitude to the steady-state one and an increase in the rate of change of fluid pressure is observed immediately after loading. The transient response of fluid pressure may have a significant effect on the mechanical behavior of poroelastic materials in various fields.

Keywords: Porous material, Poroelasticity, Transient response, Fluid pressure, Cyclic loading

1. INTRODUCTION

The application of mechanical loading on fluid-saturated porous media induces interaction between interstitial fluid flow and matrix material deformation. That is, solid-to-fluid coupling occurs when a change in applied stress produces a change in fluid pressure or a transport of interstitial fluid, while fluid-to-solid coupling occurs when fluid pressure or its transport causes a change in the volume of the matrix material. The solid-fluid interactions lead to the time-dependent mechanical behavior of the porous media. Poroelasticity (Biot, 1941, 1955) is known as the theory that quantifies the interaction between matrix deformation and fluid flow in poroelastic materials and is used to evaluate the time-dependent behavior.

Poroelasticity, which traces its origin in geomechanics, was proposed by Biot (1941, 1955) to solve soil consolidation problems. It is a coupled theory for the deformation of linear elastic materials governed by Hooke's law and fluid flow governed by Darcy's law. Example applications of the theory range from macroscopic phenomena, such as groundwater pressure fluctuations due to atmospheric pressure and earth tides (Jacob, 1940; Bredehoeft, 1967), to microscopic phenomena such as interstitial fluid flow in biological tissues (Nowinski and Davis 1970; Mow *et al*., 1980; Yang and Taber, 1991). Fluid motions play an important role in these phenomena and have been mainly focused on in the poroelastic analyses of such phenomena. To quantify the fluid flow, depending on the fluid pressure gradient, it is necessary to understand the spatial distribution and temporal fluctuation of fluid pressure.

In general, when poroelastic materials are subjected to cyclic loading, a transient state precedes a steady state in fluid pressure. Particularly under the condition of intermittent

loading, the transient response occurs frequently, and its contribution to the magnitude of the fluid flow is comparably equal to that of the steady-state response. Therefore, to understand the mechanical behavior of poroelastic materials under cyclic loading in detail, it is essential to investigate both the steady-state and transient responses. Although many researchers have focused on steady-state poroelastic behaviors under cyclic loading in geomechanics (Rojstaczer, 1988; Roeloffs, 1996) and biomechanics (Harrigan and Hamilton, 1993; Zhang and Cowin, 1994), there are no theoretical studies that focus on the transient state observed after loading application.

In this study, we present an analytical solution of interstitial fluid pressure including the transient response in poroelastic materials under cyclic uniaxial loading. Assuming the plane strain condition, the poroelastic problem is simplified to a two-dimensional problem. Based on the solution, we demonstrate how two dominant parameters, namely, a material parameter governing the solid-fluid coupling and the loading frequency, affect the distribution and evolution of fluid pressure in the poroelastic material, with particular emphasis on the transient state.

2. FORMULATION AND SOLUTION OF POROELASTIC PROBLEM

2.1 GOVERNING EQUATIONS OF POROELASTICITY

Poroelasticity (Wang, 2000) assumes that (i) Hooke's law governs the deformation of the matrix material and (ii) Darcy's law governs the fluid flow in poroelastic materials. Assuming isotropic behavior in stress-strain relations and fluid flow in poroelastic materials, the

isotropic diffusion equation for poroelasticity can be expressed using stress tensor σ_{ij} and fluid pressure p:

$$c\nabla^2\left(\sigma_{kk}+\frac{3}{B}p\right)=\frac{\partial}{\partial t}\left(\sigma_{kk}+\frac{3}{B}p\right) \quad , \tag{1}$$

where σ_{kk} represents a sum of the three normal stresses with the Einstein summation convention for repeated subscripts. Consolidation coefficient c and Skempton's coefficient B are respectively given by

$$c=\frac{k}{\mu}\left[\frac{2G(1-\nu)}{(1-2\nu)}\right]\left[\frac{B^2(1+\nu_u)^2(1-2\nu)}{9(1-\nu_u)(\nu_u-\nu)}\right] \tag{2}$$

$$B=\frac{1/K-1/K_s}{\phi/K_f+1/K-(1+\phi)/K_s} \quad , \tag{3}$$

where G is the shear modulus, K is the drained bulk modulus $K=2G(1+\nu)/3(1-2\nu)$, K_s is the bulk modulus of the solid, K_f is the bulk modulus of the fluid, ϕ is the porosity, ν is the drained Poisson's ratio, k is the permeability, and μ is the fluid viscosity. The undrained Poisson's ratio ν_u is defined by

$$\nu_u=\frac{3\nu+B(1-2\nu)(1-K/K_s)}{3-B(1-2\nu)(1-K/K_s)} \quad . \tag{4}$$

The drained condition corresponds to the situation in which the fluid pressure equilibrates with the environmental pressure, usually assumed to be zero, while the undrained condition denotes the situation in which the fluid does not move.

The stress σ_{ij} and the fluid pressure p satisfy

$$\nabla^2\left[\sigma_{kk}+\frac{2\alpha(1-2\nu)}{(1-\nu)}p\right]=0 \quad , \tag{5}$$

which is obtained from the strain compatibility equation, where α is the Biot-Willis

coefficient given by

$$\alpha = 1 - \frac{K}{K_s} \quad . \tag{6}$$

2.2 TWO-DIMENSIONAL POROELASTIC MATERIAL MODEL

We consider the two-dimensional poroelastic material model shown in Fig. 1, with a width $2a$ in the x direction and a unit thickness. This model is sandwiched between two rigid and impermeable plates at the top and bottom. The edges of the model $x = \pm a$ are stress-free and drained, that is the fluid pressure p satisfies

$$p\left(x = \pm a,\, t\right) = 0 \quad . \tag{7}$$

This boundary condition denotes that the fluid can freely leak from the edges. A cyclic axial load, $F\left(t\right) = -2ap_0 \sin \omega t$, is applied along the y direction at time $t = 0$ through the rigid plates; that is, the boundary condition for stresses is

$$\int_{-a}^{a} \sigma_{yy} dx = -2ap_0 \sin \omega t \quad , \tag{8}$$

where p_0 and ω are, respectively, the amplitude and the angular frequency of the applied stress.

2.3 ASSUMPTION OF PLANE STRAIN CONDITION

Owing to the problem symmetry, stress components and fluid pressure depend only on x and t. Assuming no shear stresses throughout the poroelastic material, that is, $\sigma_{xy}\left(x,\, t\right) = 0$, stress equilibrium requires $\sigma_{xx}\left(x,\, t\right) = 0$. Moreover, under a plane strain condition in the z direction, constitutive relations yield

$$\sigma_{kk} = (1+\nu)\sigma_{yy} - (1-2\nu)\alpha p \quad . \tag{9}$$

Substituting Eq. (9) into Eqs. (1) and (5), the diffusion equation and strain compatibility equation are respectively reduced to

$$c\frac{\partial^2}{\partial x^2}\left[\sigma_{yy} + \frac{3}{B(1+\nu_u)}p\right] = \frac{\partial}{\partial t}\left[\sigma_{yy} + \frac{3}{B(1+\nu_u)}p\right] \tag{10}$$

$$\frac{\partial^2}{\partial x^2}\left[\sigma_{yy} + \frac{\alpha(1-2\nu)}{(1-\nu)}p\right] = 0 \quad . \tag{11}$$

We introduce the following dimensionless parameters:

$$x^* \equiv \frac{x}{a}, \quad t^* \equiv \frac{ct}{a^2}$$

$$\Omega \equiv \frac{a^2\omega}{c}, \quad H = \frac{1-\nu}{\nu_u - \nu}$$

$$\sigma_{ij}^* \equiv \frac{\sigma_{ij}}{p_0}, \quad p^* \equiv \frac{p}{B(1+\nu_u)p_0/3} \quad . \tag{12}$$

Using Eq. (12), the diffusion equation Eq. (10), the strain compatibility equation Eq. (11), and the boundary conditions Eqs. (7) and (8) lead to

$$\frac{\partial^2}{\partial x^{*2}}\left(\sigma_{yy}^* + p^*\right) = \frac{\partial}{\partial t}\left(\sigma_{yy}^* + p^*\right) \tag{13}$$

$$\frac{\partial^2}{\partial x^{*2}}\left(\sigma_{yy}^* + \frac{1}{H}p^*\right) = 0 \tag{14}$$

$$p^*\left(x^* = \pm 1, t^*\right) = 0 \tag{15}$$

$$\int_{-1}^{1}\sigma_{yy}^* dx^* = -2\sin\Omega t^* \quad . \tag{16}$$

Eventually, this poroelastic problem results in the system of the partial differential equations Eqs. (13) and (14) under the boundary conditions Eqs. (15) and (16).

2.4 SOLUTION

We solve the boundary problem shown in the previous section for fluid pressure p^*.

Integration of Eq. (14) and use of Eq. (15) yield

$$\sigma_{yy}^*\left(x^*, t^*\right) = \sigma_{yy}^*\left(1, t^*\right) - \frac{1}{H} p^*\left(x^*, t^*\right) \quad . \tag{17}$$

Substituting Eq. (17) into Eq. (13) to eliminate the fluid pressure p^* leads to the following partial differential equation for σ_{yy}^*:

$$\frac{\partial^2 \sigma_{yy}^*\left(x^*, t^*\right)}{\partial x^{*2}} = \frac{\partial \sigma_{yy}^*\left(x^*, t^*\right)}{\partial t^*} + \frac{H}{1-H} \frac{\partial \sigma_{yy}^*\left(1, t^*\right)}{\partial t^*} \quad . \tag{18}$$

By taking the Laplace transform of Eq. (18) with the assumption of no stresses under the initial condition, the general solution of Eq. (18) is obtained:

$$\tilde{\sigma}_{yy}^*\left(x^*, s\right) = A(s)\cosh\sqrt{s}x^* + B(s)\sinh\sqrt{s}x^* - \frac{H}{1-H}\tilde{\sigma}_{yy}^*\left(1, s\right) \quad , \tag{19}$$

where the tilde signifies the Laplace transform, $A(s)$ and $B(s)$ are unknown coefficients to be determined from boundary conditions. Because the symmetry about $x^* = 0$ requires $B(s) = 0$, substituting $x^* = 1$ into Eq. (19) yields

$$\tilde{\sigma}_{yy}^*\left(1, s\right) = \left(1-H\right) A(s)\cosh\sqrt{s} \quad . \tag{20}$$

Therefore, substitution of Eq. (20) into Eq. (19) leads to

$$\tilde{\sigma}_{yy}^*\left(x^*, s\right) = A(s)\left\{\cosh\sqrt{s}x^* - H\cosh\sqrt{s}\right\} \quad . \tag{21}$$

Application of the Laplace transform of boundary condition Eq. (16) and use of Eq. (21) yield

$$A(s) = -\frac{\dfrac{\Omega}{s^2+\Omega^2}\sqrt{s}}{\sinh\sqrt{s} - H\sqrt{s}\cosh\sqrt{s}} \quad . \tag{22}$$

Thus, all the unknown parameters are determined.

By substituting Eqs. (20) and (21) into the Laplace transform of Eq. (17), the Laplace transform of the fluid pressure $p^*\left(x^*, t^*\right)$ is expressed as

$$\tilde{p}^*\left(x^*, s\right) = A(s) H\left\{\cosh\sqrt{s} - \cosh\sqrt{s}x^*\right\} \quad . \tag{23}$$

By applying the inverse Laplace transform of Eq. (23) with the help of Eq. (22), the fluid pressure $p^*\left(x^*, t^*\right)$ can eventually be expressed as the sum of the transient response $p^*_{trans}\left(x^*, t^*\right)$ and the steady-state response $p^*_{steady}\left(x^*, t^*\right)$ in the following form:

$$p^*\left(x^*, t^*\right) = p^*_{trans}\left(x^*, t^*\right) + p^*_{steady}\left(x^*, t^*\right) \quad . \tag{24}$$

Each term in the previous equation is

$$p^*_{trans}\left(x^*, t^*\right) = -2\sum_{n=1}^{\infty} \frac{\Omega\lambda_n^2}{\lambda_n^4 + \Omega^2} \frac{\sin\lambda_n}{\lambda_n - \sin\lambda_n\cos\lambda_n}\left(\cos\lambda_n x^* - \cos\lambda_n\right)\exp\left(-\lambda_n^2 t^*\right) \tag{25}$$

$$\begin{aligned} p^*_{steady}\left(x^*, t^*\right) &= \sin\Omega t^* - \mathrm{Im}\left[\frac{H\sqrt{i\Omega}\cosh\sqrt{i\Omega}x^* - \sinh\sqrt{i\Omega}}{H\sqrt{i\Omega}\cosh\sqrt{i\Omega} - \sinh\sqrt{i\Omega}} e^{i\Omega t}\right] \\ &= \frac{H}{K_1^2 + K_2^2}\sqrt{\frac{\Omega}{2}}\left[\left\{K_3\left(x^*\right)\left(-K_1 + K_2\right) - K_4\left(x^*\right)\left(K_1 + K_2\right)\right\}\cos\Omega t^*\right. \\ &\qquad \left. -\left\{K_4\left(x^*\right)\left(-K_1 + K_2\right) + K_3\left(x\right)\left(K_1 + K_2\right)\right\}\sin\Omega t^*\right] \quad , \end{aligned} \tag{26}$$

where λ_n is the n^{th} solution of

$$\frac{\tan\lambda_n}{\lambda_n} = H \tag{27}$$

and K_1, K_2, K_3 and K_4 are given by

$$K_1 = \cos\sqrt{\frac{\Omega}{2}}\sinh\sqrt{\frac{\Omega}{2}} - H\sqrt{\frac{\Omega}{2}}\left\{\cos\sqrt{\frac{\Omega}{2}}\cosh\sqrt{\frac{\Omega}{2}} - \sin\sqrt{\frac{\Omega}{2}}\sinh\sqrt{\frac{\Omega}{2}}\right\}$$

$$K_2 = \sin\sqrt{\frac{\Omega}{2}}\cosh\sqrt{\frac{\Omega}{2}} - H\sqrt{\frac{\Omega}{2}}\left\{\cos\sqrt{\frac{\Omega}{2}}\cosh\sqrt{\frac{\Omega}{2}} + \sin\sqrt{\frac{\Omega}{2}}\sinh\sqrt{\frac{\Omega}{2}}\right\}$$

$$K_3\left(x^*\right) = \cos\sqrt{\frac{\Omega}{2}}\cosh\sqrt{\frac{\Omega}{2}} - \cos\sqrt{\frac{\Omega}{2}}x^*\cosh\sqrt{\frac{\Omega}{2}}x^*$$

$$K_4\left(x^*\right)=\sin\sqrt{\frac{\Omega}{2}}\sinh\sqrt{\frac{\Omega}{2}}-\sin\sqrt{\frac{\Omega}{2}}x^*\sinh\sqrt{\frac{\Omega}{2}}x^* \quad . \tag{28}$$

Eqs. (24)-(28) have shown that the fluid pressure $p^*\left(x^*, t^*\right)$ depends on two dimensionless parameters, Ω and H. Hereinafter, Ω and H are called dimensionless frequency and dimensionless stress coefficient, respectively.

3. RESULTS

3.1 DISTRIBUTION AND EVOLUTION OF FLUID PRESSURE

As shown in Eqs. (24)-(28), the dimensionless fluid pressure p^* in a poroelastic material is expressed as a function of the normalized position x^* and time t^*, and depends on the dimensionless parameters Ω and H. The normalization constant of p^* defined in Eq. (12), that is, $B\left(1+\nu_u\right)p_0/3$, represents the undrained fluid pressure under constant loading, $F\left(t\right)=-2ap_0$, applied along the y direction. We can consider the undrained condition when p^* is close to 1. Thus, the dimensionless fluid pressure p^* stands for the parameter that characterizes the drainage extent. Here, we demonstrate how the parameters Ω and H affect the fluid pressure distribution and evolution.

First, we investigated the effect of the dimensionless frequency Ω on the behavior of fluid pressure $p^*\left(x^*, t^*\right)$. The fluid pressure behaviors for $\Omega = 0.1$ and 100, with $H = 50$, are shown in Figs. 2 and 3, respectively. Second, we also investigated the effect of the dimensionless stress coefficient H on p^*, for $H = 5$, 50, and 100, with $\Omega = 1$. Only the fluid pressure behaviors for $H = 5$ and 100, with $\Omega = 1$, are respectively shown in Figs. 4 and 5. Because the behaviors for $H = 50$ and 100 are almost the same, we did not show the case for

H = 50. Table 1 summarizes the set of parameters and corresponding figures. Figures (a) and (b) in Figs. 2-5 show the fluid pressure distribution across the width of the poroelastic material; (a) corresponds to the transient response plotted at t^* = 0, 0.01, and 0.1, and (b) corresponds to the steady-state response plotted for eight equal-length phase points in a period. Figures (c) and (d) in Figs. 2 and 3 respectively show the fluid pressure evolution at x^* = 0.0 and 0.8; (c) is the representative fluid pressure evolution at the point far from the material surfaces, while (d) is that at the point close to the surfaces.

3.2 EFFECT OF DIMENSIONLESS FREQUENCY Ω

The dimensionless frequency Ω defined in Eq. (12) represents the ratio of the characteristic time of the fluid pressure relaxation, $\tau_r = a^2/c$, to that of applied forces, $\tau_f = 1/\omega$. This parameter Ω was also introduced by Zhang and Cowin (1994) in their analytical study of a poroelastic beam subjected to oscillatory axial and bending loading. Although they have demonstrated the behavior of fluid pressure in the steady state due to a change in the dimensionless frequency, little attention has been paid to the transient state. In this section, we discuss in particular how the frequency Ω affects the transient response of fluid pressure.

The transient stage of fluid pressure lasts for some time after the cyclic loading is applied to the poroelastic material. The transient stage is related to the phase shift between the fluid pressure evolution in the steady state and the applied cyclic loading. As shown in Figs. 2 (c) and 2 (d), the fluid pressure evolution for Ω = 0.1 reveals that the fluid pressure phase and the loading phase do not match in the steady state due to the interstitial fluid transport. Therefore,

the steady-state fluid pressure at $t^* = 0$, $p^*_{steady}\left(x^*, 0\right)$, is not usually equal to zero. Considering that $p^*\left(x^*, 0\right)$ is always zero throughout the material because the magnitude of loading at $t^* = 0$ is zero, it is obvious that the transient response of the fluid pressure $p^*_{trans}\left(x^*, 0\right)$ bridges the gap between $p^*_{steady}\left(x^*, 0\right)$ and $p^*\left(x^*, 0\right)$. That is, the transient response offsets the steady-state response to make $p^*\left(x^*, 0\right)$ zero and eliminates the phase shift between the fluid pressure evolution and the cyclic loading immediately after loading. Thus, the transient response $p^*_{trans}\left(x^*, t^*\right)$ becomes dominant when the phase shift is substantial.

Figures 2 (a) and 3 (a) reveal that, as the dimensionless frequency Ω increases, the effect of the transient response becomes negligible around the center of the poroelastic material far from the surfaces. When Ω is less than 1, the interstitial fluid can easily drain from the material surfaces because the characteristic time of loading τ_f is larger than that of the fluid pressure relaxation τ_r. Under this condition, there is a considerable phase shift between the applied loading and the corresponding fluid pressure at each point, $x^* = 0.0$ and 0.8, in the material as shown in Figs. 2 (c) and 2 (d). As a result, the transient response occurs across the material resulting in the elimination of the phase shift. On the other hand, when Ω is higher than 1, the interstitial fluid is difficult to move, particularly around the center far from the surfaces. This is also supported by the fact that the fluid pressure gradient in the steady state around $x^* = 0.0$ for $\Omega = 100$ shown in Fig. 3 (b) is almost zero. Therefore, as shown in Figs. 3 (c) and 3 (d), the applied cyclic loading and the fluid pressure evolution are in phase around the center, while the phase shift appears only near the surfaces. In this situation with higher

frequency Ω, the effect of the transient response is limited to the region close to the surfaces of the poroelastic material.

The effect of the transient response is predominant only in the first period of the applied cyclic loading and decays immediately. Although the contribution to the magnitude of the fluid pressure by transient response is considerably small, the point we wish to emphasize is that an increase in the rate of change of fluid pressure is observed immediately after loading, as indicated by the arrow in Figs. 2 (c) and 2 (d).

3.3 EFFECT OF DIMENSIONLESS STRESS COEFFICIENT *H*

The dimensionless stress coefficient H defined in Eq. (12) is the material parameter that governs the coupling behavior between solid and fluid in poroelastic materials. When H is large, the drained Poisson's ratio ν and the undrained Poisson's ratio ν_u are almost the same because both Poisson's ratios satisfy the relation $\nu \le \nu_u \le 0.5$. As we have noted in Sec. 2.1, ν is the Poisson's ratio when the material is deformed while the fluid pressure is maintained at zero, and ν_u is that when the material is deformed in the absence of fluid transport. Therefore, when the drained and undrained Poisson's ratios are approximately the same, the fluid-to-solid coupling is weaker than the solid-to-fluid coupling in the poroelastic material, i.e., the interstitial fluid pressure has a negligible effect on the deformation of the material.

Figs. 4 and 5 show that, as the dimensionless stress coefficient H increases, the amplitude of the steady-state response decreases. In addition, the magnitude of the transient response at $t^* = 0$ also decreases to correspond to the steady-state response at zero phase. It is clear from

these facts that, when the stress coefficient H is larger, which denotes that the fluid-to-solid coupling is negligible, the amplitude of the fluid pressure evolution is smaller. Conversely, when H is smaller, which denotes that the fluid-to-solid coupling has as large an effect as the solid-to-fluid one, the amplitude of the fluid pressure evolution is larger.

As we have mentioned before, the fluid pressure behaviors for $H = 50$ and 100 are almost the same. This is because both the dimensionless stress coefficients, $H = 50$ and 100, are sufficiently large to neglect the effect of the fluid-to-solid coupling. Thus, it is obvious that, when H is larger than 50, the fluid pressure behavior under cyclic uniaxial loading depends only on the dimensionless frequency Ω.

4. DISCUSSION

In this study, we obtained an analytical solution of interstitial fluid pressure including the transient response in poroelastic materials subjected to cyclic uniaxial loading. The solution revealed that the fluid pressure behavior depends on two dimensionless parameters: the dimensionless frequency Ω that stands for the ratio of the characteristic time of the fluid pressure relaxation to that of applied forces, and the dimensionless stress coefficient H governing the solid-fluid coupling behavior in poroelastic materials. In addition, we have pointed out the following feature of the transient response of fluid pressure: when the phase shift between the applied cyclic loading and the corresponding fluid pressure evolution is large, the transient response is comparable in magnitude to the steady-state one and an increase in the rate of change of fluid pressure is observed immediately after loading.

Some transient poroelastic problems have been solved analytically thus far. For example, Terzaghi's problem, which focuses on the consolidation of a finite soil layer, and Mandel's problem, which focuses on the compression of an infinitely long and rectangular poroelastic plate, have been well known in geomechanics (Wang, 2000; Coussy, 2004). By using their analytical solutions, we can easily illustrate the time evolution of mechanical quantities of fluid-saturated poroelastic materials under Heaviside step loading conditions. Meanwhile, Zhang and Cowin (1994) presented the steady-state solution of fluid pressure evolution in a poroelastic beam subjected to oscillatory axial and bending loading. Assuming the absence of bending, free leakage at surfaces, and plane strain condition in their problem, their analysis conditions reduce to those of our work. Consequently, our steady-state solution, Eq. (26), is almost the same as Eq. (25), for the case $m = 0$, $\eta \to \infty$, in their study (Zhang and Cowin, 1994). Furthermore, other theoretical studies have clarified the mechanical behaviors of poroelastic materials under cyclic loading in geomechanics (Rojstaczer, 1988; Roeloffs, 1996) and biomechanics (Harrigan and Hamilton, 1993). They have presented steady-state solutions of interstitial fluid pressure for different boundary value problems. However, little attention has been paid to the transient stage observed immediately after the application of cyclic loading, and there are no theoretical studies that focus on this phenomenon. Therefore, we have focused on the transient response and derived the complete time history of fluid pressure under cyclic loading.

The interstitial fluid pressure behavior shown in this study is commonly observed in various poroelastic materials under cyclic loading. For instance, the behavior of living bone,

which contains a bone matrix and interstitial fluid, can be modeled as a poroelastic material. Based on poroelastic analyses, many researchers have investigated the interaction between the bone matrix and the interstitial fluid (Cowin, 1999). The interstitial fluid flow induced by bone matrix deformation is considered to play an important role in cellular mechanosensing as well as in the transport of nutrients (Burger and Klein-Nulend, 1999). Weinbaum *et al*. (1994) proposed a hypothesis that the osteocytes, which are embeded in the bone matrix and surrounded by interstitial fluid, are stimulated by fluid-induced shear stresses acting on their osteocytic processes.

In this paper, we particularly focused on bone trabeculae, in which boundary conditions of force and loading frequency are important factors. As for boundary conditions of force, the poroelastic materials in the practical problems are usually under complex loading conditions: they are subjected to bending and shearing loading as well as axial loading simultaneously. Among them, the axial loading condition shows us the basic and primary mechanical features of poroelastic materials. In addition, considering the widely recognized hypothesis that the trabecular architecture of bone matches the stress trajectories as a result of bone remodeling (Wolff, 1986), it seems reasonable to assume that trabeculae *in vivo* are predominantly under axial loading. The relationship between trabecular orientation and stress distribution is investigated by bone remodeling simulation (Adachi *et al*., 2001; Tsubota *et al*., 2002). On the other hand, the trabeculae are subjected to physiological cyclic loading owing to locomotion and posture. By using the loading frequency ranging from 1 to 20 Hz (Weinbaum *et al*., 1994) and material parameters of trabeculae estimated by Smit *et al*. (2002) and Beno *et al*. (2005),

the dimensionless frequency Ω which trabeculae experience in daily activity is derived as 10^{-2}-10^{2}. This order of the magnitude covers the range of dimensionless frequencies used in our study. It follows from what has been discussed that it is meaningful to extend our solution to the analysis of the mechanical behavior of trabeculae.

We emphasize that the transient stage observed immediately after the application of cyclic loading is important for bone remodeling. This transient start to the steady state was also confirmed using a finite element procedure (Manfredini *et al*., 1999). In the study, it was reported that the duration of the transient stage was confined almost in the first cycle of the loading curve, which agrees with our result. Despite its fast decay, the transient response is accompanied by an increase in the rate of change of fluid pressure. Meanwhile, it was suggested that adaptive processes attributed to bone remodeling can be engendered by intermittent loading rather than repetitive activity for long periods (Rubin and Lanyon, 1984). In addition, it was also reported that the dominant factor that enhances bone growth was the strain rate rather than the strain magnitude (O'Connor *et al*., 1982; Lanyon and Rubin, 1984). Following these studies, if we assume that the osteocytic response to mechanical stimuli depends on the rate of change in fluid shear stress as well as its magnitude, it is reasonable to suggest that the transient response may have a significant effect on bone growth.

This study has shown that a poroelastic material in the transient state portrays a unique mechanical behavior which is characteristically different from that in the steady state. Moreover, the contribution of the transient response of fluid pressure under noncyclic loading, such as impulse or step loading, is more significant than that under cyclic loading. Thus,

focusing on the transient response revealed by poroelastic analysis may enable us to gain new insights for future studies on geomechanics and biomechanics.

ACKNOWLEDGEMENT

This work was partly supported by the Grant-in-Aid for Scientific Research from the Ministry of Education, Culture, Sports, Science and Technology of Japan, and by the 21st Century COE Program for Research and Education on Complex Functional Mechanical Systems at Kyoto University.

REFERENCES

Adachi, T., Tsubota, K., Tomita, Y., Hollister, S.J., 2001. Trabecular surface remodeling simulation for cancellous bone using microstructural voxel finite element models. ASME J. Biomech. Eng. 123 (5), 403-409.

Beno, T., Yoon, Y.J., Cowin, S.C., Fritton, S.P., 2006. Estimation of bone permeability using accurate microstructural measurements. J. Biomech. 39 (13), 2378-2387.

Biot, M.A., 1941. General theory of three-dimensional consolidation. J. Appl. Phys. 12 (2), 155-164.

Biot, M.A., 1955. Theory of elasticity and consolidation for a porous anisotropic solid. J. Appl. Phys. 26 (2), 182-185.

Bredehoeft, J.D., 1967. Response of well-aquifer systems to earth tides. J. Geophys. Res. 72 (12), 3075-3087.

Burger, E.H., Klein-Nulend, J., 1999. Mechanotransduction in bone - role of the lacuno-canalicular network. FASEB J. 13, S101-S112.

Coussy, O., 2004. Poro Mechanics. John Wiley & Sons, Ltd, England, 298p.

Cowin, S.C., 1999. Bone poroelasticity. J. Biomech. 32 (3), 217-238.

Harrigan, T.P., Hamilton, J.J., 1993. Bone strain sensation via transmembrane potential changes in surface osteoblasts: loading rate and microstructural implications. J. Biomech. 26 (2), 183-200.

Jacob, C.E., 1940. On the flow of water in an elastic artesian aquifer. Trans. Am. Geophys. Union 22, 783-787.

Lanyon, L.E., Rubin, C.T., 1984. Static vs dynamic loads as an influence on bone remodeling. J. Biomech. 17 (12), 897-905.

Manfredini, P., Cocchetti, G., Maier, G., Redaelli, A., Montevecchi, F.M., 1999. Poroelastic finite element analysis of a bone specimen under cyclic loading. J. Biomech. 32 (2), 135-144.

Mow, V.C., Kuei, S.C., Lai, W.M., Armstrong, C.G., 1980. Biphasic creep and stress-relaxation of articular-cartilage in compression: thory and experiments. J. Biomech. Engng 102 (1), 73-84.

Nowinski, J.L., Davis, C.F., 1970. A model of the human skull as a poroelastic spherical shell subjected to a quasistatic load. Math. Biosci. 8, 397-416.

O'Connor, J.A., Lanyon, L.E., Macfie, H., 1982. The influence of strain rate on adaptive bone remodeling. J. Biomech. 15 (10), 767-781.

Roeloffs, E.A., 1996. Poroelastic techniques in the study of earthquake-related hydrologic phenomena. Adv. Geophys. Academic Press Inc, San Diego, pp. 135-195.

Rojstaczer, S., 1988. Determination of fluid-flow properties from the response of water levels in wells to atmospheric loading. Water Resour. Res. 24 (11), 1927-1938.

Rubin, C.T., Lanyon, L.E., 1984. Regulation of bone formation by applied dynamic loads. J. Bone Joint Surg. 66A (3), 397-402.

Smit, T.H., Huyghe, J.M., Cowin, S.C., 2002. Estimation of the poroelastic parameters of cortical bone. J. Biomech. 35 (6), 829-835.

Tsubota, K., Adachi, T., Tomita, Y., 2002. Functional adaptation of cancellous bone in human proximal femur predicted by trabecular surface remodeling simulation toward uniform stress state. J. Biomech. 35 (12), 1541-1551.

Wang, H.F., 2000. Theory of Linear Poroelasticity with Applications to Geomechanics and Hydrogeology. Princeton Univ. Press, Princeton, 287p.

Weinbaum, S., Cowin, S.C., Zeng, Y., 1994. A model for the excitation of osteocytes by mechanical loading-induced bone fluid shear stresses. J. Biomech. 27 (3), 339-360.

Wolff, J., 1986. The law of bone remodeling. (Trans. P. Maquet and R. Furlong), Springer

Yang, M., Taber, L.A., 1991. The possible role of poroelasticity in the apparent viscoelastic behavior of passive cardiac muscle. J. Biomech. 24 (7), 587-597.

Zhang, D., Cowin, S.C., 1994. Oscillatory bending of a poroelastic beam. J. Mech. Phys. Solids 42 (10), 1575-1599.

FIGURES

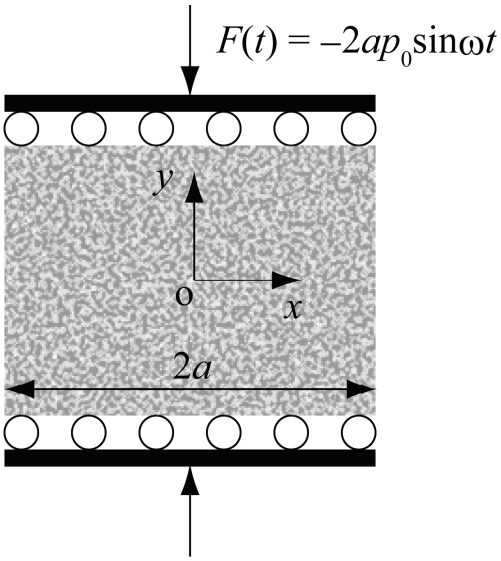

Fig. 1: Two-dimensional trabecular model subjected to a cyclic loading.

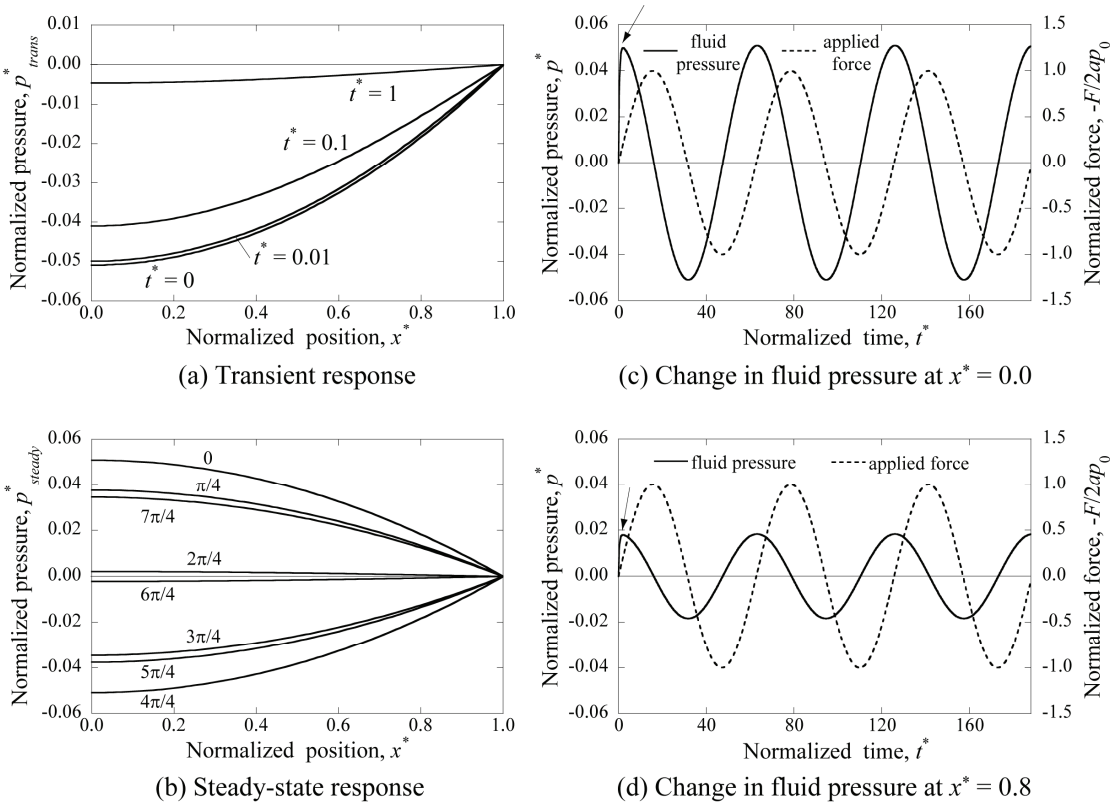

(a) Transient response

(c) Change in fluid pressure at $x^* = 0.0$

(b) Steady-state response

(d) Change in fluid pressure at $x^* = 0.8$

Fig. 2: Fluid pressure behavior for $H = 50$, $\Omega = 0.1$.

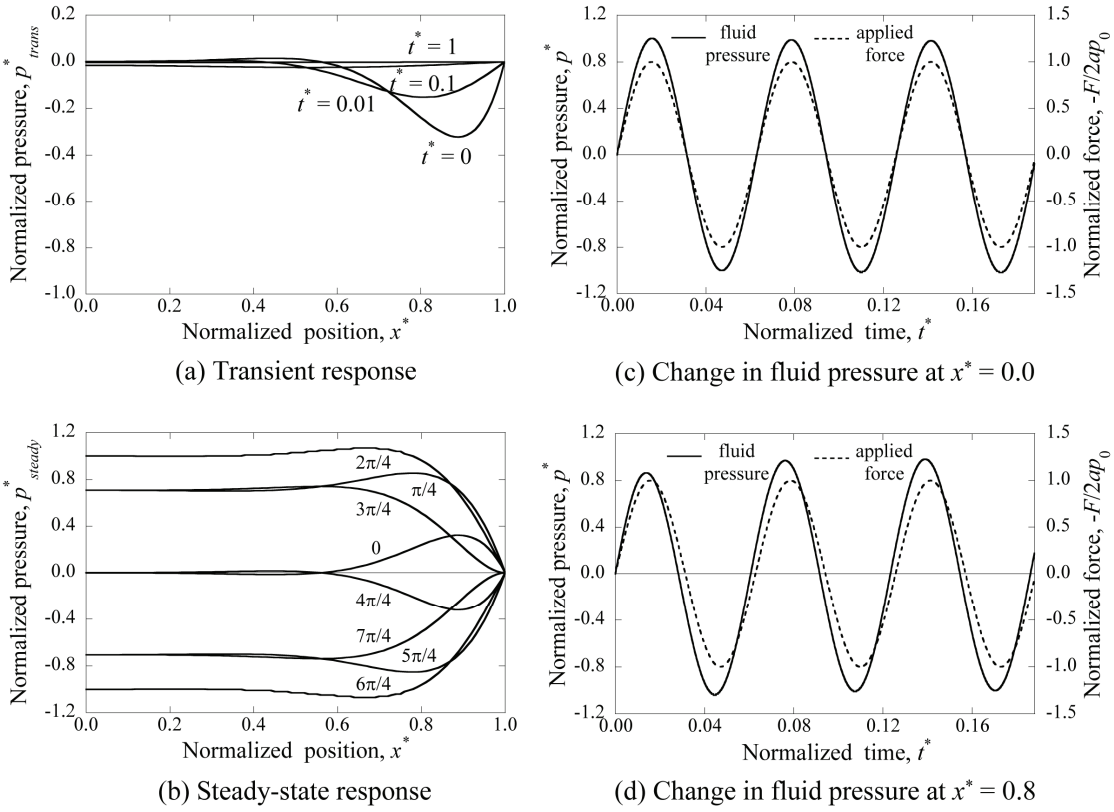

(a) Transient response

(c) Change in fluid pressure at $x^* = 0.0$

(b) Steady-state response

(d) Change in fluid pressure at $x^* = 0.8$

Fig. 3: Fluid pressure behavior for $H = 50$, $\Omega = 100$.

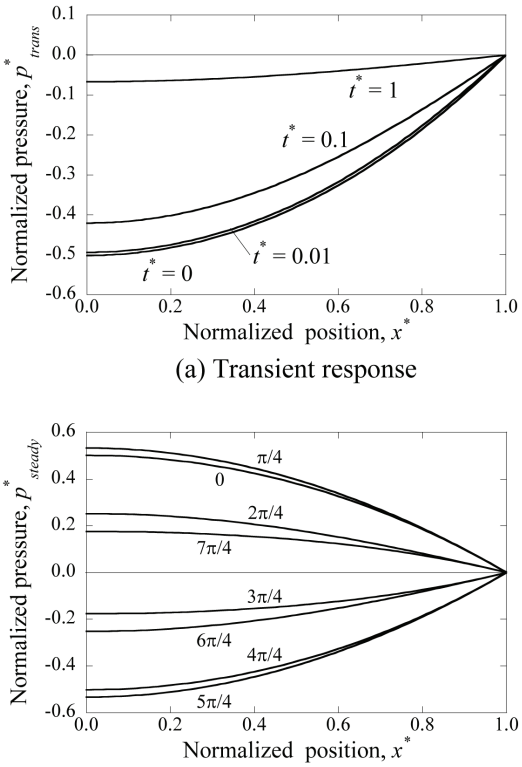

(a) Transient response

(b) Steady-state response

Fig. 4: Fluid pressure distribution for $\Omega = 1$, $H = 5$.

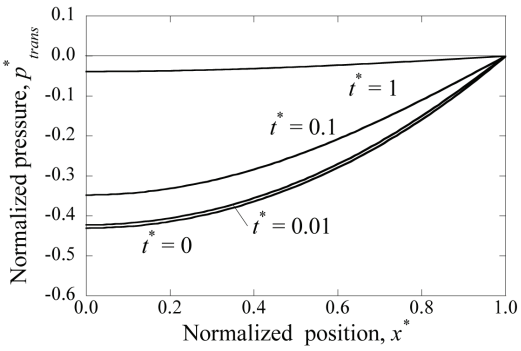

(a) Transient response

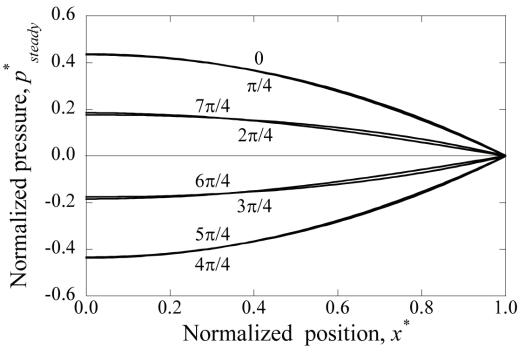

(b) Steady-state response

Fig. 5: Fluid pressure distribution for $\Omega = 1$, $H = 100$.

TABLE

Table 1: Parameters and corresponding figures. Because the fluid pressure behaviors for $H =$ 50 and 100, with $\Omega = 1$, are almost the same, only the case for $H = 100$ is shown in Fig. 5.

H \ Ω	0.1	1	100
5		Fig. 4	
50	Fig. 2	(Fig. 5)	Fig. 3
100		Fig. 5	